JTEP Jurnal Keteknikan Pertanian,
Vol. 14 No. 2, p 212-226, 2026
P-ISSN 2407-0475 E-ISSN 2338-8439

Available online:
http://journal.ipb.ac.id/index.php/jtep
DOI: 10.19028/jtep.014.2.212-226

Research Article

OPEN ACCESS Check for updates

Kalman Filter Stabilization of Multi-Sensor Water Quality Measurements under Turbulent Flow in Eel Aquaculture

Ahmad Zambarkah Sarwo Surono[1], Herry Suhardiyanto[2*], I Dewa Made Subrata[2],Yonvitner[3,4]

[1]Agricultural Engineering Study Program, Faculty of Engineering and Technology, IPB University, Indonesia.
[2]Division of Biosystems Engineering, Faculty of Engineering and Technology, IPB University, Indonesia.
[3]Department of Aquatic Resources Management, Faculty of Fisheries and Marine Sciences, IPB University, Indonesia.
[4]Centre for Coastal and Marine Resources Studies, IPB University, Indonesia.
*Corresponding author, email: herrysuhardiyanto@apps.ipb.ac.id

Article Info

Submitted: 6 March 2026
Revised: 11 May 2026
Accepted: 6 june 2026
Available online: 11 June 2026
Published: June 2026

Keywords:
Eel environment, Kalman filter, Noise reduction, Unsteady flow, Water quality.

How to cite:
Surono, A. Z. S. S., Suhardiyanto, H., Subrata. I. M., Yonviter. (2026). Kalman Filter Stabilization of Multi-Sensor Water Quality Measurements under Turbulent Flow in Eel Aquaculture. Jurnal Keteknikan Pertanian, 14(2): 212-226.
https://doi.org/*10.19028/jtep.014.212-226.*

Abstract

While Kalman Filters are widely used for water quality sensors, most studies focus on static environments, ignoring hydrodynamic noise in continuous-flow systems such as eel aquaculture, where turbulence-induced sensor instability may directly affect automated control decisions. This study evaluated the performance of the Kalman Filter in mitigating multi-sensor reading noise caused by unsteady flow from a wavemaker in a closed aquarium. Experiments simulated an eel environment (salinity 5-7 ppt, flow velocity 0.27 m/s) to measure pH, electrical conductivity (EC), dissolved oxygen (DO), and water temperature in situ. The performance of the Kalman Filter was compared directly with the that of Simple Moving Average (SMA), Exponentially Weighted Moving Average (EWMA), and Butterworth filters. The performance of these filters was assessed using the Standard Deviation, Root Mean Square Error (RMSE), Noise Reduction Ratio (NRR), Signal-to-Noise Ratio (SNR), and Smoothness Index. The results demonstrate that the Kalman Filter not only reduces signal fluctuations but also improves measurement accuracy, as validated by lower RMSE values relative to ground truth references under static conditions. It outperformed the other algorithms by reducing the average standard deviation by 87.65%, lowering the mean RMSE by 28.22%, decreasing the average noise by 13.56%, and increasing the mean SNR by 4.44 dB. This study demonstrates the superiority of the Kalman Filter in stabilizing sensor data against complex hydrodynamic turbulence.

Doi: https://doi.org/10.19028/jtep.014.2.212-226

1. Introduction

Eels (Anguilla spp.) contain 17.51% protein and 17.72% fat (Nafsiyah et al., 2018), along with significant concentrations of unsaturated fatty acids, specifically DHA and EPA (6.31% /100 g) (Emi

Available online:
http://journal.ipb.ac.id/index.php/jtep
DOI: 10.19028/jtep.014.2.212-226

Widyasari et al., 2014). Furthermore, the vitamin A content in eels is remarkably high, reaching 2068 μg/100 g, which surpasses the levels found in both Bulgarian black sea and horse mackerel (Wijayanti & Setiyorini, 2018). In addition to their high nutritional value, eels have a high economic value that continues to increase annually. Based on empirical data from industry practitioners, the price trends for eel seeds (glass eel phase) are presented in Table 1.

Table 1. Glass Eel pricing trend (in a thousand).

Years	2008	2015	2016	2017	2018	2019	2020
Price (Rp/kg)	700	1.500	1.800	2.300	2.800	3.300	3.500

Despite promising economic returns, eel aquaculture remains constrained by the fact that the supply of glass eel seeds is entirely dependent on wild-caught stock. Furthermore, the survival rate (SR) during the initial rearing phase remains critically low, ranging between 50% and 60% (Affandi, 2016). This stems from the high sensitivity of larvae to environmental fluctuations; consequently, maintaining ideal water quality is a primary concern, and ensuring dynamic water circulation is essential to mimic natural habitat conditions and mitigate stress in the fish (Shao et al., 2021). Given these complexities, a precise and real-time monitoring mechanism is imperative, particularly because current eel aquaculture practices still rely heavily on manual water quality monitoring and nonautomated control systems for pH regulation, salinity adjustment, and aeration management.

Current technological advancements, particularly in sensor technology, have enabled more precise and sustainable water quality monitoring (Parra et al., 2018), and the integration of the Internet of Things (IoT) has facilitated real-time data acquisition (Huang & Khabusi, 2025). Furthermore, contemporary measurement applications increasingly employ multi-sensor systems to achieve higher accuracy, comprehensive datasets, consistent readings, and overall system reliability (Gao et al., 2016). Water quality sensors, such as those for pH, dissolved oxygen (DO), and electrical conductivity (EC), operate with low-level electrical signals, making them highly susceptible to electromagnetic interference (EMI) and signal coupling, which can lead to measurement fluctuations and biases (Yaroshenko et al., 2020). Furthermore, the natural habitat of eels requires continuous water flow; however, this turbulence can affect the dissolved oxygen distribution, pH gradients, and physical characteristics of the fluid surrounding the sensors. These factors introduce significant noise into the response and compromise the accuracy of the water quality readings (Reimers & Fogaren, 2021). Consequently, these challenges necessitate a systemic approach capable of minimizing noise in the sensor responses to ensure data integrity.

While conventional filtration techniques, such as the Simple Moving Average (SMA)(Svetunkov & Petropoulos, 2018), Exponential Weight Moving Average (EWMA)(Sukparungsee et al., 2020), and Infinite Impulse Response (IIR) Butterworth filters (Shouran & Elgamli, 2020), are frequently

Available online:
http://journal.ipb.ac.id/index.php/jtep
DOI: 10.19028/jtep.014.2.212-226

employed to mitigate turbulence-induced noise, they often introduce phase lagging or signal overshoot. To overcome these limitations, this study proposes a predictive Kalman Filter that optimally suppresses fluctuations by integrating system dynamics with uncertainty variance (Christakis et al., 2024). Despite its proven efficacy, existing validations are predominantly limited to stagnant-water conditions. Consequently, a critical research gap remains regarding the empirical analysis of sensor distortion caused by dynamic mechanical noise and the capability of predictive algorithms to mitigate this interference.

To address the aforementioned research limitations, this study tested a multi-sensor water quality system directly under the influence of artificial flow turbulence generated by a wavemaker. The primary objective was to comparatively evaluate the reliability of the Kalman Filter algorithm against conventional filters, such as the SMA, EWMA, and Butterworth, in suppressing turbulence-induced noise in multi-sensor water quality measurements. Furthermore, this study investigated the implications of signal stabilization on threshold-based automated control systems for aquaculture applications.

Unlike previous studies that mainly focused on static water environments or single-sensor evaluations, this study experimentally investigated the performance of multi-sensor water quality measurements under controlled turbulent flow conditions that represent realistic eel aquaculture environments. The novelty of this study lies in the integration of turbulence-induced sensor noise analysis, comparative evaluation of multiple filtering algorithms (Kalman, SMA, EWMA, and Butterworth), and evaluation of their implications for automated control systems involving pH dosing, salinity dosing, and aeration.

2. Material and Methods

Research activities were conducted from October 2025 to January 2026. The experiments were conducted at the Siswadhi Soepardjo Field Laboratory, Faculty of Engineering and Technology, IPB University.

2.1 Experimental Design and Environmental

Data acquisition for this study was conducted in an experimental aquarium measuring 100 cm in length, 40 cm in width, and 50 cm in height (with an effective water depth of 25 cm). An air stone and a wavemaker were installed at one end of the aquarium, as illustrated in Figure 1. To characterize the hydrodynamic environment, flow velocity profiles were established at four distinct distances from the wavemaker (25, 35, 45 cm, and 55 cm).

A wavemaker was selected to generate controlled and repeatable flow conditions that simulated realistic aquatic environments. This approach has been widely used to produce calibrated flow velocities for evaluating eel swimming behavior, supporting its applicability in controlled hydrodynamic studies (Linda et al., 2023).

JTEP Jurnal Keteknikan Pertanian,
Vol. 14 No. 2, p 212-226, 2026
P-ISSN 2407-0475 E-ISSN 2338-8439
Available online:
http://journal.ipb.ac.id/index.php/jtep
DOI: 10.19028/jtep.014.2.212-226

The multi-sensor module was positioned 35 cm from the wavemaker to ensure consistent exposure to turbulent flow conditions while minimizing excessive flow fluctuations that could distort the sensor measurements.

The physical water parameters within the experimental aquarium were regulated to replicate the optimal rearing conditions for eels in the glass eel and elver stages, as established in prior studies (Table 2). Prior to experimentation, the initial water quality conditions were established using filtered rain-harvesting water and adjusted to meet the target ranges specified in Table 2. All parameters were stabilized under no-flow (static) conditions to ensure a consistent baseline before initiating the flow-based measurement. This procedure ensured that the variations observed during the experiment were primarily influenced by hydrodynamic conditions rather than initial water quality fluctuations.

Table 2. Water Quality Design Criteria.

Parameter	Ideal Set Point	Source
Water Acidity	7.0 - 8.0	(Handajani et al., 2024)
Dissolved Oxygen	65% - 80%	(Taqwa et al., 2018)
Total Dissolved Solid	22.5 - 76.25 ppm	(Tahiluddin et al., 2025)
Water Salinity	8.3 ppt	(Lukas et al., 2017)
Water Temperature	28 - 30 °C	(Fekri et al., 2018)
Water Turbidity	30 - 40 cm	(Santosh & Singh, 2017)
Water Flow Velocity	0.2 – 0.6 m/s	(Linda et al., 2023)

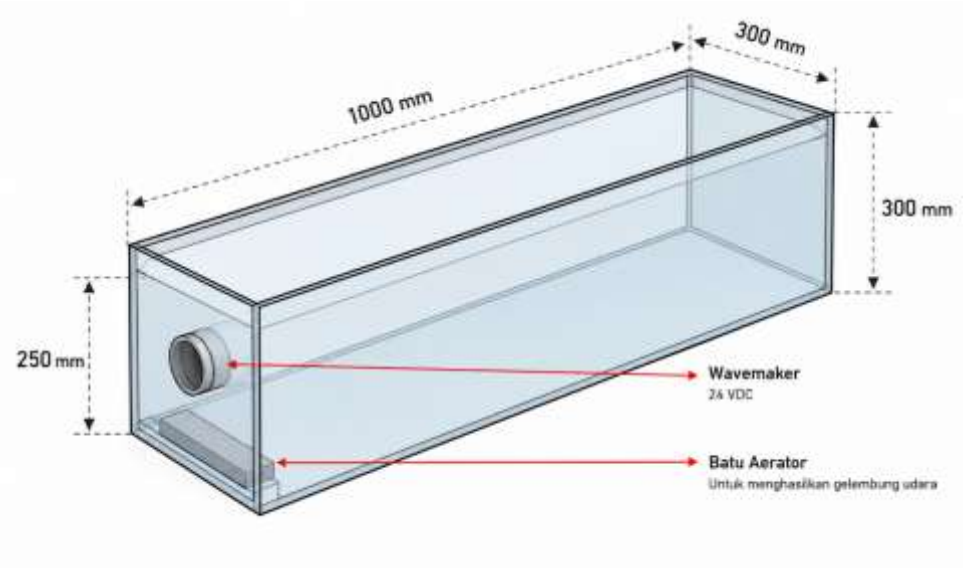

Figure 1. Experimental setup design.

JTEP Jurnal Keteknikan Pertanian,
Vol. 14 No. 2, p 212-226, 2026
P-ISSN 2407-0475 E-ISSN 2338-8439
Available online:
http://journal.ipb.ac.id/index.php/jtep
DOI: 10.19028/jtep.014.2.212-226

2.2 Multi-Sensor Module Design

The aquaculture monitoring system utilized an integrated multisensor approach, consisting of pH, DO, EC, and temperature (DS18B20 type) measurement instruments. All the sensor probes were arranged circularly in a cylindrical module to ensure that the turbulent flow profile exposure received by each sensor membrane surface was uniform. The instrument module was centrally connected to an ESP32 microcontroller via a multiplexing mechanism. This mechanism was designed to allow the sequential activation of each instrument's reading, thereby significantly suppressing electrical interference (crosstalk) between the sensors in the conductive medium.

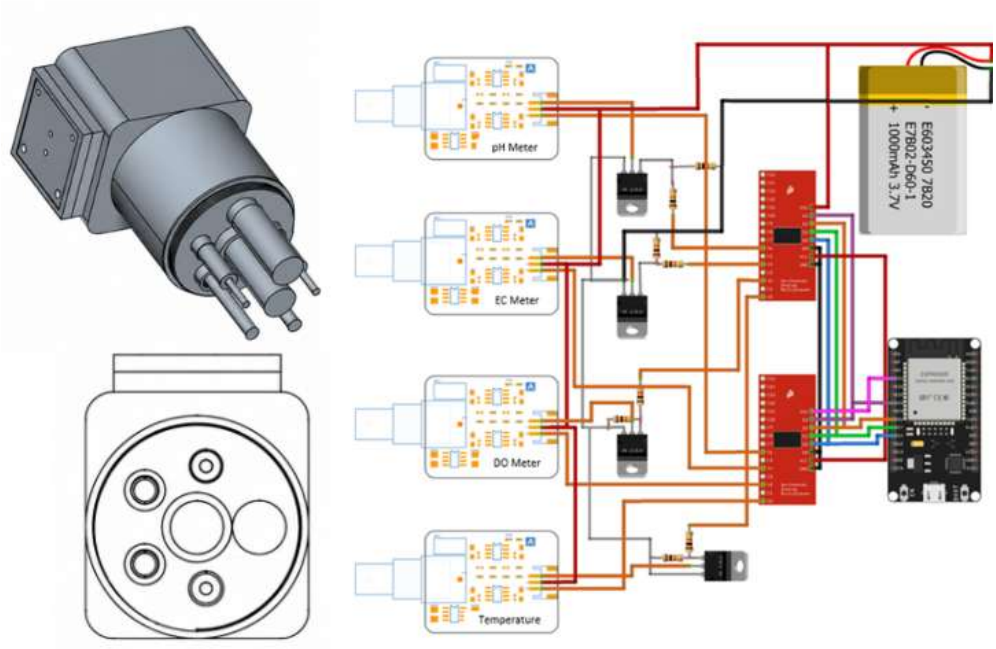

Figure 2. 3D design of the sensor module and electronic schematic design.

2.3 Sensor Calibration

The pH sensor was calibrated by recording the analog values of the sensor when immersed in several standardized buffer solutions with pH levels of 4.0, 4.01, 6.86, 7.00, 9.18, and 10.0. The analog value was plotted on the X-axis, whereas the actual pH buffer value served as the Y-axis. The plotted points generated a regression line accompanied by a mathematical function and determination coefficient (R2). Consequently, a pH calibration equation was established with an R2 value of 0.9954.

$$Value_{(pH)} = -0.0048 * Value_{(Sensor)} + 15.249 \quad (1)$$

The calibration of the EC sensor against salinity solutions was conducted by preparing 10 different salinity concentrations, ranging from 1 ppt to 10 ppt using sea salt (e.g., 1 ppt equals 1 g of salt per

Available online:
http://journal.ipb.ac.id/index.php/jtep
DOI: 10.19028/jtep.014.2.212-226

liter of water). The sensor was immersed in each solution, and the corresponding analog values were recorded and plotted to obtain a linear regression equation with an R2 of 0.9921

$$Salinity\ Value_{(ppt)} = 0.0024 * Value_{Sensor} - 0.235 \quad (2)$$

The analog output of the DO sensor was converted into a Dissolved Oxygen percentage (%) based on the calibration equation. Calibration was performed by immersing the probe in a Sodium Sulfite (Na2SO3) solution, which intrinsically has a zero DO level, to record the absolute lower limit of the sensor. The probe was then exposed to atmospheric air until the analog reading stabilized, establishing the upper limit for 100% oxygen saturation. This calibration process yielded the following equation:

$$\%\ Dissolved\ Oxygen = \frac{(y_{baca} - y_{(DO=0)})}{(y_{(DO=100)} - y_{(DO=0)})}\ x\ 100 \quad (3)$$

Water temperature is a critical parameter that significantly affects the physical properties of aquatic environments. Higher water temperatures inherently reduce the solubility of DO, thereby affecting DO measurements. In addition, according to the DFRobot sensor specifications, the pH, EC, and DO measurements are temperature-dependent and may require temperature compensation to maintain measurement accuracy (DFRobot, 2024). Therefore, all calibration and experimental procedures in this study were conducted within a controlled water temperature range of 26.8–27.8 °C to minimize deviations in thermal measurements.

2.4 Filter Parameter Configuration

The implementation of signal-filtering algorithms requires the configuration of filter constants to achieve an optimal balance between noise reduction and signal responsiveness. The specific configurations of these filtering constants are presented in Table 3.

Table 3. Filter Configuration

Parameter	Ground Truth	SMA	EWMA	*Butterworth*	Kalman
pH	7.00	N=200	0.001	f_s=50, f_c=0.01	Q=0.00001
EC (ppt)	5.21	N=200	0.001	f_s=50, f_c=0.01	Q=0.00001
D0 (%)	92.28	N=200	0.001	f_s=50, f_c=0.01	Q=0.00001
Temperature (*C)	26.00	N=200	0.005	f_s=50, f_c=0.005	Q=0.0005

2.5 Dynamic Flow Characteristics Analysis

As a supporting metric, the fluid flow regime hitting the instrument placement area was verified for its turbulence dynamicity level using a dimensionless parameter, the Reynolds Number (Re), as shown in Equation. (4).

Available online:
http://journal.ipb.ac.id/index.php/jtep
DOI: 10.19028/jtep.014.2.212-226

$$Re = \frac{\rho v(t) L}{\mu} = \frac{v(t) L}{v} \quad (4)$$

Where ϱ = Water density (kg/m³), $v(t)$= Total fluid flow velocity in the sensor placement area (m/s), L = Characteristic length of the test system (m), μ = Dynamic fluid viscosity (Pa·s), , v = Kinematic Viscosity.

2.6 Sensor Response Measurement under Flow Disturbance

To observe the influence of flow on the pH, EC, DO, and temperature sensors, an additional module was developed to measure the current consumption of the wavemaker as an indicator of its OFF and ON states. The system simultaneously recorded the responses of each sensor and the current signal of the wavemaker. Data acquisition was initiated at 0 s under static conditions with the wavemaker turned off and continued until 69 s. The wavemaker was then activated at 70 s to generate a turbulent flow, and the measurements continued until 300 s, at which point the entire system was stopped.

Subsequently, the mean values and standard deviations of the sensor outputs were calculated under both the wavemaker OFF and ON conditions. The sensor signals were visually analyzed to identify flow-induced delays and fluctuations, with three repeated trials conducted for each parameter.

2.7 Predictive Approach (Kalman Filter)

The Kalman Filter algorithm was implemented recursively to suppress fluctuations in the aquatic signal without reducing the sensor's responsiveness (i.e., avoiding signal attenuation). This filter operation is divided into two sequential processes: the forecast (predict) and adjustment (update) stages. The projected system condition estimate is calculated based on the noise variance track record according to Equation. (5) and (6).

$$\hat{x}^{-}(k) = \hat{x}(k-1) \quad (5)$$

$$P^{-}(k) = P(k-1) + Q \quad (6)$$

The second stage actively updates the Kalman Gain (K) calculation adaptively to validate the projected estimate with the latest in-situ sensor reading figures according to Equation. (7)–(9).

$$K(k) = \frac{P^{-}(k)}{P^{-}(k)+R} \quad (7)$$

$$\hat{x}(k) = \hat{x}^{-}(k) + K(k)[z(k) - \hat{x}^{-}(k)] \quad (8)$$

$$P(k) = (1 - K(k))P^{-}(k) \quad (9)$$

Where x ^- *(k)* = Predicted estimate of water quality parameter, *P*^- *(k)* = Error covariance matrix from the prediction stage, Q = Process noise, R = Measurement noise, K(k) = Kalman Gain, *z(k)* = Raw data voltage signal read at time k.

JTEP Jurnal Keteknikan Pertanian,
Vol. 14 No. 2, p 212-226, 2026
P-ISSN 2407-0475 E-ISSN 2338-8439
Available online:
http://journal.ipb.ac.id/index.php/jtep
DOI: 10.19028/jtep.014.2.212-226

2.8 Comparative Conventional Filters

To evaluate the performance of the proposed Kalman Filter, several conventional filtering algorithms were implemented for comparison, including the SMA, EWMA, and a second-order Butterworth low-pass filter.

The implemented second-order Butterworth filtering equation is expressed in Equation. (10).

$$Butterworth_t = b_0.x_t + b_1.x_{t-1} + b_3.x_{t-2} - a_1.y_{t-1} - a_2.y_{t-2} \quad (10)$$

The SMA and EWMA filtering equations are formulated as follows: (11) and (12).

$$SMA_t = \frac{1}{N}\sum_{i=1}^{N} X_{i-1} \quad (11)$$

$$EWMA_t = \alpha X_t + (1-\alpha)EWMA_{t-1} \quad (12)$$

where N = Moving average window size, and α is the exponentially weighted smoothing parameter ($0 < \alpha < 1$).

2.9 ON-OFF Control System Evaluation

A threshold-based ON–OFF control strategy was implemented for aeration, pH dosing, and salinity dosing. The aerator was activated when the dissolved oxygen level fell below the predefined set point and deactivated once the target value was reached. Similarly, the salinity dosing pump operated whenever the measured salinity was below the desired set point.

For pH regulation, a time-based dosing strategy was applied to allow the pH sensor readings to stabilize after the chemical injection. When the measured pH value was below the target set point, the dosing pump was activated for 13 s, followed by a stabilization period of 167 s, before the next control evaluation cycle. This approach was implemented to reduce the rapid fluctuations in pH measurements caused by mixing and sensor response delays after dosing.

The control system performance was evaluated by comparing the use of raw sensor signals and Kalman-filtered signals as the control inputs. During the experiments, the actuator current consumption and sensor outputs were recorded simultaneously to observe the influence of signal stabilization on the actuator activation behavior in the aeration, pH dosing, and salinity dosing systems.

2.10 Performance Evaluation Parameters

The accuracy deviation of each filter architecture was statistically evaluated using the Root Mean Square Error (RMSE) and Signal-to-Noise Ratio (SNR) parameters. The signal reading error evaluation calculation (RMSE) refers to the absolute deviation distance between the algorithm output signal and the ground truth reference level under static water test conditions, as shown in Equation. (13).

$$RMSE = \sqrt{\frac{1}{N}\sum_{k=1}^{N}\left(\hat{x}(k) - x_{ref}(k)\right)^2} \quad (13)$$

JTEP Jurnal Keteknikan Pertanian,
Vol. 14 No. 2, p 212-226, 2026
P-ISSN 2407-0475 E-ISSN 2338-8439
Available online:
http://journal.ipb.ac.id/index.php/jtep
DOI: 10.19028/jtep.014.2.212-226

In addition to RMSE, the measurement stability and noise attenuation performance were evaluated using the Standard Deviation (SD), Noise Reduction Ratio (NRR), and Smoothness Index (SI). The standard Deviation indicates the dispersion of the data relative to its mean, where a smaller SD value signifies a more stable sensor reading. It was calculated using the following equation:

$$\sigma = \sqrt{\frac{1}{N}\sum_{k=1}^{N}(x(k) - \bar{x})^2} \quad (14)$$

Where x(k)= The data value at time k, and $\bar{x}$= The mean value of the data. The NRR was used to evaluate the effectiveness of the filter in suppressing noise by comparing the variance of the raw signal with that of the filtered signal. The results are presented logarithmically, where a higher positive value indicates superior noise reduction performance. The NRR value according to Friebe and Jenau (2024) is shown in Equation. (15).

$$NRR = 10.log\left(\frac{\text{Variance of the raw data}}{\text{Variance of the filtered output data}}\right) \quad (15)$$

The success index of eliminating wave ripples (turbulent fluctuations) without distorting the original information, described as SNR, is the ratio between the average of the useful signal power and the average of the interference power (Friebe & Jenau, 2024). The SNR was calculated using Equation (16).

$$SNR = 10.\log\left(\frac{N.(Nilai\ real)^2}{\sum(Data\ Sensor - Nilai\ real)^2}\right) \quad (16)$$

Furthermore, the SI was employed to determine the filter's capability to flatten and linearize the fluctuating data. According to Hu et al. (2013), the Smoothness Index is defined as follows:. (17).

$$Smoothness = \frac{\sum(y_{filter}[i+1] - y_{filter}[i])^2}{\sum(y_{raw}[i+1] - y_{raw}[i])^2} \quad (17)$$

Data analysis was conducted to determine the filtering approach that minimized the measurement noise and improved the signal stability under turbulent flow conditions.

3. Results and Discussion

3.1 Flow Characteristics

The detailed flow velocity distributions are presented in Table 4. The flow velocity reached 0.47 m/s at a distance of 25 cm from the wavemaker and gradually decreased as the distance increased. The multi-sensor module was positioned 35 cm from the wavemaker, corresponding to a flow velocity of 0.27 m/s. At this position, the pH, EC, DO, and temperature sensors exhibited the smallest measurement deviations between the static and flow conditions under the same water characteristics.

JTEP Jurnal Keteknikan Pertanian,
Vol. 14 No. 2, p 212-226, 2026
P-ISSN 2407-0475 E-ISSN 2338-8439
Available online:
http://journal.ipb.ac.id/index.php/jtep
DOI: 10.19028/jtep.014.2.212-226

Therefore, this region was considered to provide the most stable and representative turbulent flow conditions for evaluating the sensor performance and filtering algorithms.

Table 4. Wavemaker Speed to Flow Velocity.

Position	25 cm	35 cm	45 cm	55 cm
Speed m/s	0,47	0,27	0,07	0,02

3.2 Reynolds Number

Positioning the sensor 35 cm from the wavemaker implied that the module was subjected to a flow velocity of 0.27 m/s. Consequently, the calculated dimensionless Reynolds number (Re) of 73,500 indicated a turbulent flow regime.

3.3 Sensor Response under Tutbulent Flow

As shown in Table 5, the presence of flow caused a decrease in the mean values of the pH, EC, and DO sensors, whereas the temperature sensor remained relatively unaffected. The standard deviation values, which represent the measurement noise in the sensor signals, increased under flow conditions. In addition to the changes in the mean values and standard deviations, a delay in the signal period was also observed in the pH and DO measurements, as shown in Figure 3. These alterations in sensor characteristics, including shifts in the mean values, increased noise, and signal period delays, may negatively affect the accuracy and performance of automated control systems.

Table 5. Sensor response in turbulent flow.

Parameters	Average Value		Standard Deviation	
	Without flow	With flow	Without flow	With flow
pH	6.820	6.753	0.439	0.532
EC	4.816	4.771	0.019	0.045
DO	98.392	97.764	0.282	0.551
Suhu	26.030	26.058	0.094	0.088

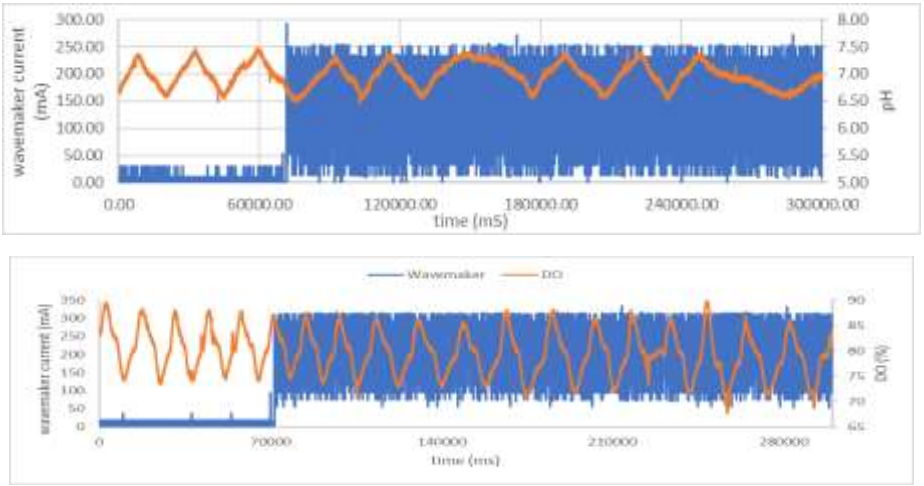

Figure 3. pH and DO sensor responses to flow disturbance.

JTEP Jurnal Keteknikan Pertanian,
Vol. 14 No. 2, p 212-226, 2026
P-ISSN 2407-0475 E-ISSN 2338-8439
Available online:
http://journal.ipb.ac.id/index.php/jtep
DOI: 10.19028/jtep.014.2.212-226

3.4 Performance Evaluation of Filter Algorithms

The quantitative performance of the filters in mitigating flow-induced noise was evaluated using statistical parameters, including RMSE, NRR, and SNR. Table 6 presents a comprehensive performance comparison among the Kalman Filter, SMA, EWMA, and Butterworth.

Table 6. Filter performance evaluation result

		SD	RMSE	SI	NRR	SNR
pH	RAW	0.166	0.2556	-	-	31.765
	SMA	0.159	0.2610	3.46E+00	0.38	31.583
	EWMA	0.043	0.1811	1.43E-05	11.66	34.757
	Butterworth	0.025	0.1727	2.11E-06	16.34	35.168
	Kalman	0.023	0.1721	3.02E-06	17.30	35.197
EC	RAW	0.010	0.5742	-	-	22.170
	SMA	0.003	0.5773	1.53E+01	10.40	22.124
	EWMA	0.002	0.5745	5.28E-07	15.09	22.165
	Butterworth	0.003	0.5751	5.53E-08	10.38	22.157
	Kalman	0.002	0.5760	1.17E-07	14.57	22.143
DO	RAW	0.303	0.3771	-	-	50.787
	SMA	0.117	0.2535	3.52E-05	8.26	54.238
	EWMA	0.046	0.2354	6.98E-07	16.37	54.880
	Butterworth	0.041	0.2571	2.47E-08	17.42	54.117
	Kalman	0.035	0.2165	1.43E-07	18.63	55.607
Temp	RAW	0.085	0.1106	-	-	50.459
	SMA	0.007	0.0708	4.73E-05	0.44	54.333
	EWMA	0.005	0.0703	1.21E-05	2.27	54.397
	Butterworth	0.005	0.0703	5.07E-08	2.83	54.392
	Kalman	0.005	0.0693	4.82E-06	3.74	54.520

Based on the evaluation metrics, the Kalman Filter consistently outperformed the other filters in almost all test scenarios. For the pH, DO, and temperature sensors, the Kalman Filter emerged as the best-performing algorithm. It demonstrated exceptional noise-filtering capabilities by reducing the standard deviation by 86.35% for the pH sensor data, 88.29% for the DO sensor data, and 94.64% for the temperature sensor data. Furthermore, it achieved NRR values of 17.30, 18.63, and 3.74 dB for the pH, DO, and temperature sensors, respectively. The Kalman Filter also significantly enhanced the data accuracy and stability by decreasing the RMSE by 32.65%, 42.69 %, and 37.34% for the pH, DO, and temperature sensors, respectively. Additionally, it successfully improved the signal clarity by increasing the SNR by 10.81%, 9.49 %, and 8.05% for the pH, DO, and temperature data, respectively. In the evaluation of the EC sensor, the EWMA filter demonstrated superior noise filtration to the Kalman Filter. It reduced the standard deviation by 82.40% (compared to 81.31% by the Kalman Filter) and yielded a higher NRR of 15.09% (compared to 14.57% by the Kalman Filter).

JTEP Jurnal Keteknikan Pertanian,
Vol. 14 No. 2, p 212-226, 2026
P-ISSN 2407-0475 E-ISSN 2338-8439
Available online:
http://journal.ipb.ac.id/index.php/jtep
DOI: 10.19028/jtep.014.2.212-226

The Kalman Filter effectively improves signal stability under turbulent flow conditions, providing a more reliable basis for automated control in aquaculture systems. This is particularly relevant for DO regulation using aerators and dosing control for pH and salinity, where unstable sensor readings may trigger unnecessary actuation responses. By reducing signal fluctuations, the Kalman Filter enhances control efficiency and system stability. However, the slight variation observed for EC indicates that the filtering performance depends on the signal characteristics. Therefore, the Kalman Filter can be applied as a primary method, with parameter-specific or hybrid filtering strategies recommended for further optimization.

3.5 Implications for Automated Control System

Figure 4 illustrates the influence of signal stabilization on the threshold-based ON–OFF control systems. The use of Kalman-filtered signals consistently reduced the actuator activation frequency and operating duration compared with the raw sensor data.

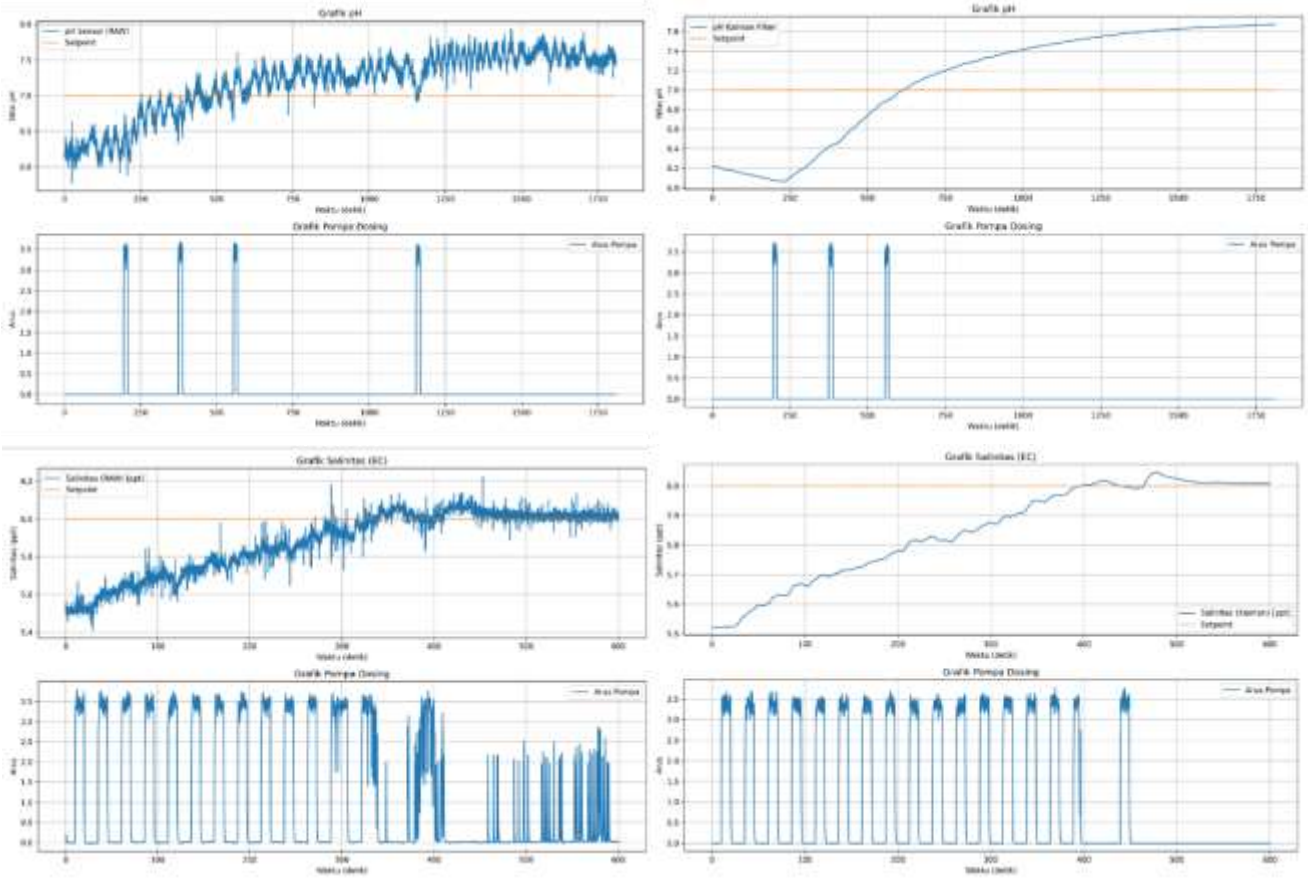

Continue

Available online:
http://journal.ipb.ac.id/index.php/jtep
DOI: 10.19028/jtep.014.2.212-226

Continue

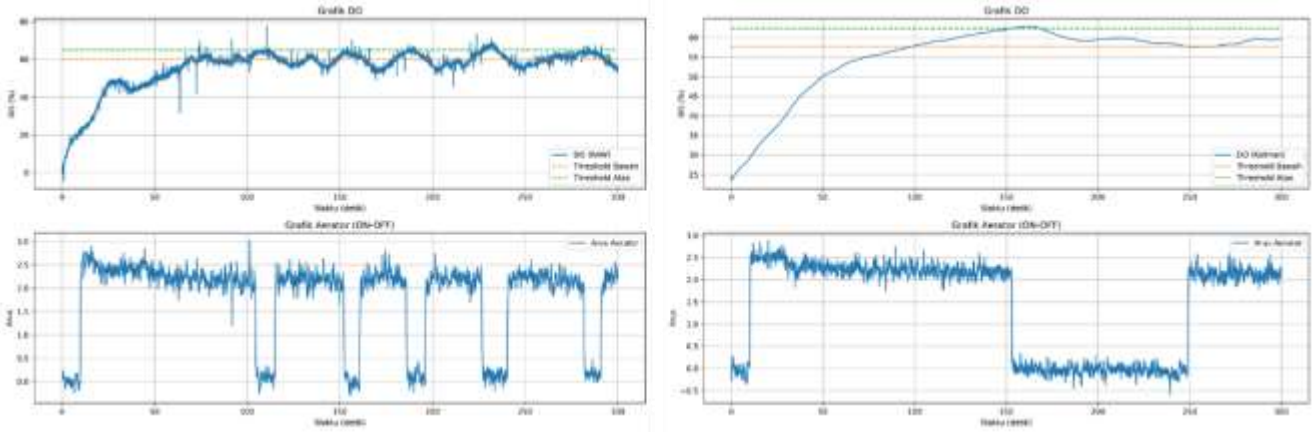

Figure 4. Comparison of control systems using raw data and Kalman filtered data

4. Conclusion

This study demonstrated that turbulence generated by continuous flow significantly degrades the stability and accuracy of multi-sensor water quality measurements. The comparative evaluation confirmed that the Kalman Filter provided the most consistent overall performance among the tested methods (SMA, EWMA, and Butterworth), particularly for turbulence-sensitive parameters such as pH and DO. Quantitatively, the Kalman Filter reduced the average standard deviation by 87.65%, decreased the RMSE by 28.22%, reduced the noise levels by 13.56%, and increased the SNR by 4.07 dB, indicating a substantial improvement in the measurement reliability under dynamic conditions.

Although slight variations were observed for EC, where the EWMA showed marginally better performance, the overall difference remained small. These findings indicate that the Kalman Filter can be effectively applied as a primary filtering approach to improve sensor accuracy in dynamic aquaculture environments. From a practical perspective, the use of the Kalman Filter provides a more reliable basis for automated control systems, such as aeration control for dissolved oxygen and dosing systems for pH and salinity. Therefore, it is recommended to implement the Kalman Filter as a baseline method.

In addition, the use of Kalman-filtered data improved the operational stability of the aerator control system, pH dosing pump, and salinity dosing pump by reducing the frequency and duration of actuator activation.

5. AI Writing Statement

The author used the Gemini generative AI tool and Google Translate as the language translator to optimize the grammar and structure, and to change the background of the figure of the experimental setup and multi-sensor module 3D design from grey color to a white background. The entire

Available online:
http://journal.ipb.ac.id/index.php/jtep
DOI: 10.19028/jtep.014.2.212-226

manuscript was written according to the author's concept in Bahasa for the first time before being translated into the English Version.

6. References

Affandi, R. (2016). Pengembangan sumberdaya ikan sidat di indonesia. In M. S. Baskoro (Ed.), teknologi pengembangan perikanan dan kelautan untuk memperkuat ketahanan pangan serta memacu perekonomian nasional secara berkelanjutan. PT Penerbit IPB Press.

Christakis, I., Tsakiridis, O., Kandris, D., & Stavrakas, I. (2024). A kalman filter scheme for the optimization of low-cost gas sensor measurements. Electronics (Switzerland), 13(1). https://doi.org/10.3390/electronics13010025

Emi Widyasari, R. A. H., Kusharto, C. M., Budywiryawan, B., Sri Wiyono, E., & Sugengherisuseno, S. (2014). Nutritive value and fatty acids profile of fresh Indonesian eel (Anguilla bicolor) and Kabayaki. Jurnal Sains Kesihatan Malaysia, 12(1), 41–46. https://doi.org/10.17576/jskm-1201-2014-06

Fekri, L., Affandi, R., Rahardjo, M. F., Budiardi, T., Simanjuntak, C. P. H., Fauzan, T., & Indrayani, I. (2018). The effect of temperature on the physiological condition and growth performance of freshwater eel elver Anguilla bicolor. Jurnal Akuakultur Indonesia, 17(2), 181. https://doi.org/10.19027/jai.17.2.181-190

Friebe, K., & Jenau, F. (2024). Evaluation Study on Wavelet Denoising of Antenna-Based PD Measurements in Strong Interference Environments Considering a New Reliability Score of Pulse Detection. IEEE Transactions on Dielectrics and Electrical Insulation, 31(6), 2887–2896. https://doi.org/10.1109/TDEI.2024.3374243

Gao, W., Emaminejad, S., Nyein, H. Y. Y., Challa, S., Chen, K., Peck, A., Fahad, H. M., Ota, H., Shiraki, H., Kiriya, D., Lien, D. H., Brooks, G. A., Davis, R. W., & Javey, A. (2016). Fully integrated wearable sensor arrays for multiplexed in situ perspiration analysis. Nature, 529(7587), 509–514. https://doi.org/10.1038/nature16521

Handajani, H., Hermawan, D., & Jasmine, A. S. (2024). Growth performance of eel fish (Anguilla bicolor) which are maintained in containers of different colors. Acta Aquatica: Aquatic Sciences Journal, 143–148. https://doi.org/10.29103/aa.v11i2.15205

Huang, Y. P., & Khabusi, S. P. (2025). Artificial intelligence of things (aiot) advances in aquaculture: A Review. In Processes (Vol. 13, Number 1). Multidisciplinary Digital Publishing Institute (MDPI). https://doi.org/10.3390/pr13010073

Hu, S., Hu, Y., Wu, X., Li, J., Xi, Z., & Zhao, J. (2013). Research of signal de-noising technique based on wavelet. In Telkomnika (Vol. 11, Number 9).

Available online:
http://journal.ipb.ac.id/index.php/jtep
DOI: 10.19028/jtep.014.2.212-226

Linda, F., Mawardi, W., Purbayanto, A., Komaruddin, D., Pemanfaatan, D., Perikanan, S., Perikanan, F., & Kelautan, I. (2023). Swimming capabilities of elver eels (Anguila bicolor) for optimal utilization of fishways. ALBACORE, 7(3), 427–436. https://doi.org/10.29244/core.7.3.427-436

Lukas, A. Y. H., Djokosetiyanto, D., Budiardi, T., Sudrajat, A. O., & Affandi, R. (2017). Optimization of salinity and calcium on Indonesian shortfin eel Anguilla bicolor maintenance (Vol. 10). http://www.bioflux.com.ro/aacl

Nafsiyah, I., Nurilmala, M., & Abdullah, A. (2018). Nutrient composition of eel anguilla bicolor bicolor and anguilla marmorata. JPHPI, 21, 19. https://doi.org/10.17844/jphpi.v21i3.24733

Parra, L., Lloret, G., Lloret, J., & Rodilla, M. (2018). Physical sensors for precision aquaculture: A Review. IEEE Sensors Journal, 18(10), 3915–3923. https://doi.org/10.1109/JSEN.2018.2817158

Reimers, C. E., & Fogaren, K. E. (2021). Bottom boundary layer oxygen fluxes during winter on the oregon shelf. journal of geophysical research: Oceans, 126(3). https://doi.org/10.1029/2020JC016828

Santosh, B., & Singh, N. P. (2017). Guidelines for water quality management for fish culture in Tripura. https://www.researchgate.net/publication/320322935

Shao, D., Huang, L., Wang, R. Q., Gualtieri, C., & Cuthbertson, A. (2021). Flow turbulence characteristics and mass transport in the near-wake region of an aquaculture cage net panel. Water (Switzerland), 13(3). https://doi.org/10.3390/w13030294

Shouran, M., & Elgamli, E. (2020). Design and Implementation of Butterworth Filter. International Journal of Innovative Research in Science, Engineering and Technology. www.ijirset.com

Sukparungsee, S., Areepong, Y., & Taboran, R. (2020). Exponentially weighted moving average—Moving average charts for monitoring the process mean. PLoS ONE, 15(2). https://doi.org/10.1371/journal.pone.0228208

Svetunkov, I., & Petropoulos, F. (2018). Old dog, new tricks: a modelling view of simple moving averages. International Journal of Production Research, 56(18), 6034–6047. https://doi.org/10.1080/00207543.2017.1380326

Tahiluddin, A. B., Bornales, J. C., Limbaro, G. R. A., Paudac, M. A. T. U., Amarille, R. K., Sirad, N. R., Kabirun, M. C., Ujing, R. A., Gonzaga-Torino, F. M., Sabdani, M. H., Bacla-An, R. E., Hairal, M. A. J. S., Magcanta-Mortos, M. L. M., & Esguerra, J. P. (2025). Environmental Impacts of Aquaculture in the Philippines. Israeli Journal of Aquaculture - Bamidgeh, 77(2), 51–81. https://doi.org/10.46989/001c.133778

Taqwa, F. H., Supriyono, E., Budiardi, T., Utomo, N. B. P., & Affandi, R. (2018). Optimization of physiological status of glass eel (Anguilla bicolor bicolor) for transport by salinity and temperature acclimatization 1,2 (Vol. 11). http://www.bioflux.com.ro/aacl

Wijayanti, I., & Setiyorini, E. S. S. (2018). Nutritional Content of wild and cultured eel (anguilla bicolor) from southern coast of central java. Ilmu kelautan: Indonesian Journal of Marine Sciences, 23(1), 37. https://doi.org/10.14710/ik.ijms.23.1.37-44

Available online:
http://journal.ipb.ac.id/index.php/jtep
DOI: 10.19028/jtep.014.2.212-226

Yaroshenko, I., Kirsanov, D., Marjanovic, M., Lieberzeit, P. A., Korostynska, O., Mason, A., Frau, I., & Legin, A. (2020). Real-time water quality monitoring with chemical sensors. In Sensors (Switzerland) (Vol. 20, Number 12, pp. 1–22). MDPI AG. https://doi.org/10.3390/s20123432